BIOCHEMISTRY
including biophysical chemistry & molecular biology

Article

pubs.acs.org/biochemistry

Identification of the GPR55 Antagonist Binding Site Using a Novel Set of High-Potency GPR55 Selective Ligands

Evangelia Kotsikorou,[†] Haleli Sharir,[‡] Derek M. Shore,[§] Dow P. Hurst,[§] Diane L. Lynch,[§] Karla E. Madrigal,[§] Susanne Heynen-Genel,[§,∥] Loribelle B. Milan,[∥] Thomas D. Y. Chung,[∥] Herbert H. Seltzman,[⊥] Yushi Bai,[@] Marc G. Caron,[@] Larry S. Barak,[@] Mitchell P. Croatt,[§] Mary E. Abood,[‡] and Patricia H. Reggio*[,§]

[†]Department of Chemistry, University of Texas-Pan American, Edinburg, Texas 78539, United States

[‡]Center for Substance Abuse Research, Temple University, Philadelphia, Pennsylvania 19140, United States

[§]Center for Drug Discovery, University of North Carolina Greensboro, Greensboro, North Carolina 27402, United States

[∥]Conrad Prebys Center for Chemical Genomics, Sanford-Burnham Medical Research Institute, La Jolla, California 92037, United States

[⊥]Center for Organic and Medicinal Chemistry, Research Triangle Institute, Research Triangle Park, North Carolina 27709, United States

[@]Department of Cell Biology, Duke University, Durham, North Carolina 27708, United States

Supporting Information

ABSTRACT: GPR55 is a class A G protein-coupled receptor (GPCR) that has been implicated in inflammatory pain, neuropathic pain, metabolic disorder, bone development, and cancer. Initially deorphanized as a cannabinoid receptor, GPR55 has been shown to be activated by non-cannabinoid ligands such as L-α-lysophosphatidylinositol (LPI). While there is a growing body of evidence of physiological and pathophysiological roles for GPR55, the paucity of specific antagonists has limited its study. In collaboration with the Molecular Libraries Probe Production Centers Network initiative, we identified a series of GPR55 antagonists using a β-arrestin, high-throughput, high-content screen of ~300000 compounds. This screen yielded novel, GPR55 antagonist chemotypes with IC_{50} values in the range of 0.16−2.72 μM [Heynen-Genel, S., et al. (2010) Screening for Selective Ligands for GPR55: Antagonists (ML191, ML192, ML193) (Bookshelf ID NBK66153; PMID entry 22091481)]. Importantly, many of the GPR55 antagonists were completely selective, with no agonism or antagonism against GPR35, CB1, or CB2 up to 20 μM. Using a model of the GPR55 inactive state, we studied the binding of an antagonist series that emerged from this screen. These studies suggest that GPR55 antagonists possess a head region that occupies a horizontal binding pocket extending into the extracellular loop region, a central ligand portion that fits vertically in the receptor binding pocket and terminates with a pendant aromatic or heterocyclic ring that juts out. Both the region that extends extracellularly and the pendant ring are features associated with antagonism. Taken together, our results provide a set of design rules for the development of second-generation GPR55 selective antagonists.

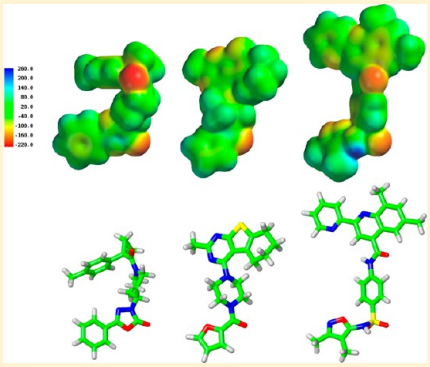

GPR55, a rhodopsin-like (class A) G protein-coupled receptor (GPCR), is a receptor for L-α-lysophosphatidylinositol (LPI), which has the potential to become an important therapeutic target (GenBank entry NM005683).[1] GPR55 has been proposed to be a cannabinoid receptor because it binds a subset of CB1 and CB2 ligands. GPR55(−/−) knockout mouse studies[2,3] have suggested a role for GPR55 in inflammatory pain, neuropathic pain, and bone development. Other studies indicate that activation of GPR55 is pro-carcinogenic.[4−7] While GPR55 shares some ligands with the cannabinoid receptors (see refs 1, 8, and 9), we and others have identified additional agonist ligands with novel chemotypes for GPR55.[10−12]

One reason for the lack of more potent and selective GPR55 ligands is that initial ligand searches were conducted using cannabinoid receptor/lipid-biased compound libraries.[12,13] Therefore, discovering and characterizing novel GPR55 chemotypes is a crucial next step in the field. This should lead to the design of higher-quality GPR55 ligands that will become new research tools or novel new drugs. In collaboration with the Molecular Libraries Probe Production Centers Network initiative, we identified a series of GPR55 antagonists using a β-arrestin, high-throughput, high-content screen of ~300000 compounds. This screen yielded novel, GPR55 antagonist chemotypes with IC_{50} values in the range of 0.16−

Received: July 6, 2013
Revised: October 27, 2013
Published: November 25, 2013

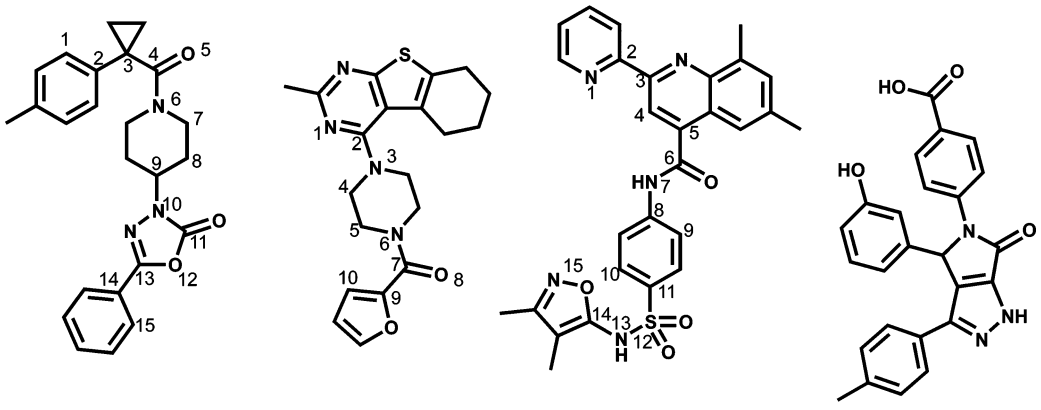

Figure 1. GPR55 antagonist structures. ML191, ML192, and ML193 are the focus of this work. CID16020046 is another GPR55 antagonist recently described[48] by Kargl and co-workers.

2.72 μM [Heynen-Genel, S., et al. (2010) Screening for Selective Ligands for GPR55: Antagonists (ML191, ML192, ML193) (Bookshelf ID NBK66153; PMID entry 22091481)] that belong to unreported GPR55 antagonist chemotypes.[11] Importantly, many of these ligands were completely selective, with no observed agonism or antagonism against GPR35, CB1, or CB2 up to 20 μM. This work focuses on three GPR55 antagonists identified in this screen (and nominated as probe compounds for future studies): ML191 (CID23612552), ML192 (CID1434953), and ML193 (CID1261822) (see Figure 1 for structures).

We previously published a refined homology model of the GPR55 activated state (GPR55 R*) and its subsequent use in exploring the interaction between GPR55 and the novel GPR55 compounds identified in our agonist screen.[14] We report here the development of a refined homology model of the GPR55 inactive state and the binding conformations of ML191, ML192, and ML193 at GPR55. Our modeling identifies a common binding region despite the chemical diversity of their scaffolds as well as those portions of each molecule that render it an antagonist. Taken together, our results provide a set of design rules for the development of second-generation, highly selective GPR55 antagonists.

METHODS

Chemical Library Screening. A β-arrestin (see below), high-throughput, high-content screen (HCS) of 300000 compounds was used here to identify potent GPR55 selective antagonists. This work was performed in collaboration with the Molecular Libraries Probe Production Centers Network program.[11] For more details about this library of compounds, see http://mli.nih.gov/mli/compound-repository/mlsmr-compounds/. Compounds were screened for antagonism (PubChem AID 2026) at GPR55 (using LPI as the agonist), as well as for both agonism and antagonism at GPR35 (PubChem AIDs 2809 and 2815), CB1 (PubChem AIDs 2814 and 2835), and CB2 (PubChem AIDs 2822 and 2836). A cell line permanently expressing a β-arrestin GFP biosensor and an enhanced receptor of interest (i.e., GPR55, GPR35, CB1, or CB2) were employed in the high-content imaging assay. Assay protocol descriptions (according to AID number) can be accessed at the PubChem Web site (http://pubchem.ncbi.nlm.nih.gov/). Potent GPR55 antagonist compounds that lacked agonism or antagonism at GPR35, CB1, or CB2 were further evaluated for inhibition of pERK activation and PKCβII translocation produced by the GPR55 agonists, LPI or ML186 (see below). A set of novel GPR55 antagonist molecular scaffolds were selected from the screen of ML191 (CID23612552), ML192 (CID1434953), and M193 (CID1261822), and the binding of each compound was explored using a computer model of the GPR55 inactive state (see below).

Biochemical Studies. LPI (Sigma-Aldrich), ML191, ML192, ML193, and ML186 (MolPort) were dissolved in dimethyl sulfoxide to a concentration of 10 mM; 10 mM stock solutions were dissolved in Hanks' balanced salt solution (HBSS) to working concentrations.

β-Arrestin Translocation. U2OS cells permanently expressing HA-GPR55E and βarr2-GFP have been previously described.[15] Cells were seeded onto glass coverslips at 80–85% confluence and placed in 24-well plates (BD Falcon). Cells were maintained at 37 °C in 5% CO_2 overnight. Cells were washed briefly with HBSS before the application of the drug. Experiments were performed using HBSS (Fisher Scientific) as the assay buffer. Agonist-stimulated redistribution of βarr2-GFP was assessed following a 40 min drug treatment at room temperature (RT). Cells were then fixed with 4% paraformaldehyde for 25 min at room temperature followed by three washes with PBS and one wash with doubly distilled water. The antagonism protocol included preincubation with the antagonist for 15 min, followed by a 40 min co-application with the agonist.

The high-throughput protocol for identifying small antagonists molecules has been previously described[11] (PubChem AID 2026).

Quantification of Data. The RGB color images captured from the fluorescent microscope were transformed into eight-bit grayscale images using the Automate-Batch function in Adobe Photoshop CS5. To quantify βarr2-GFP aggregates, grayscale images were processed via ImageJ (http://rsbweb.nih.gov/ij/), using a custom-written plug-in.[16] Inhibition curves were analyzed by nonlinear regression using GraphPad Prism version 5.0 (GraphPad, San Diego, CA), and data were fit to sigmoidal concentration–response curves to obtain IC_{50} values. Activity values were normalized to the maximal response achieved by agonist (ML186 or LPI).

dx.doi.org/10.1021/bi4008885 | *Biochemistry* 2013, 52, 9456–9469

PKCβII Translocation Assay of GPR55 Activation. HEK-293 cells plated in 35 mm glass well Matek plastic dishes were transiently transfected with 175 μL of a solution containing 1.5 μg/mL PKCβII-GFP cDNA or the PKC plasmid and 5 μg/mL human GPR55 cDNA in pCMV-Sport6 (Open Biosystems, Huntsville, Al) using a standard calcium phosphate protocol. Cells expressing GPR55 and PKCβII-GFP were utilized 24 h after transfection. Cells were washed with warm MEM and maintained at 37 °C in 5% CO_2 for 30−45 min after the application of the drug. Inhibition of agonist-stimulated redistribution of PKCβII-GFP was assessed after drug treatment at RT.

Extracellular Signal-Regulated Kinase 1/2 Assays. Extracellular signal-regulated kinase 1/2 phosphorylation was assessed by immunoblotting, as previously described.[17] GPR55E-expressing U2OS cells were grown to subconfluence in 60 mm plates and serum-starved overnight before the assay. Cells were rinsed once with HBSS, and antagonist compounds were applied for 30 min prior to agonist application (10 μM LPI, 10 min). Following drug treatment, the cells were disrupted in lysis buffer [50 mM Hepes, 150 mM NaCl, 1 mM EDTA, 1 mM EGTA, 10% glycerol, 1% Triton X-100, 10 μM $MgCl_2$, 20 mM *p*-nitrophenyl phosphate, 1 mM Na_3VO_4, 25 mM NaF, and a protease inhibitor mixture (1:25, pH 7.5)]. Lysates were immediately placed on ice for 10 min and then centrifuged at 16000*g* for 30 min at 4 °C. Supernatants, corresponding to the cytosolic fraction, were collected, and protein concentrations were determined by the Bradford assay (Bio-Rad) using bovine serum albumin as a standard. Cytosolic fractions (20 μg) were separated on a 10% gel by sodium dodecyl sulfate−polyacrylamide gel electrophoresis followed by immunoblotting. Antibodies against doubly phosphorylated ERK1/2 (1:5000) were detected using a LI-COR Odyssey IR Imager (LI-COR Biotechnologies, Lincoln, NE). A polyclonal antibody against total ERK1/2 (Cell Signaling 9102, 1:1000) was used to confirm equal protein loading. Densitometric analysis was performed using a LI-COR Odyssey IR Imager. The value obtained for both ERK1 and ERK2 was normalized to total ERK1/2 levels. The data were normalized to the response achieved by 10 μM LPI and are presented as percent inhibition.

Receptor Model Development. The construction of our initial GPR55 receptor homology model was described previously by Kotsikorou et al.[17] This homology model used the crystal structure of β_2-AR (Protein Data Bank entry 2RH1)[18] as the template. This initial model has been modified to reflect several structural elements found in the X-ray crystal structure of CXCR4 in its inactive state, a receptor with which the GPR55 receptor shares a high degree of homology.[19] (1) TMH2 and TMH4 of GPR55 were modeled using the corresponding helices in the CXCR4 structure. GPR55 and CXCR4 have prolines at positions 2.58 and 4.59 that would lead to very different conformations of TMH2 and TMH4 compared to the β_2-AR template that has prolines at positions 2.59 and 4.60. In addition, preceding the prolines at positions 2.56 and 4.57, CXCR4 has threonines in a g^- conformation that influence the overall bend of each helix. Analogously, GPR55 has serines at positions 2.56(76) and 4.57(153) that can assume a g^- conformation. Therefore, the use of CXCR4 TMH2 and TMH4 as templates is well-justified. (2) The high degree of sequence homology between GPR55 and CXCR4 at the extracellular ends of TMH6 and TMH7 dictated the introduction of extracellular (EC) helical extensions into the EC3 loop of GPR55 to match that of CXCR4. (3) The EC-2 loop in CXCR4 contains a β sheet. Because of the high degree of sequence similarity in this region, as well, the β sheet motif was built into the EC-2 loop in GPR55. (4) In addition to the disulfide bridge between the EC-2 loop and C3.25, CXCR4 has another disulfide bridge between a Cys in the N-terminus Cys(28) and Cys(274) in the EC-3 loop. The same residues [Cys(10) and Cys(260)] are found in the GPR55 sequence, so this second disulfide bridge was added to the GPR55 model. The GPR55 inactive state model is also characterized by an intracellular hydrogen bond between R3.50(119) and Q6.30(221) that closes off the intracellular domain of the receptor, preventing G protein interaction.

The resultant homology model was energy-minimized using the OPLS 2005 force field in Macromodel version 9.9 (Schrödinger Inc., Portland, OR). An 8.0 Å extended nonbonded cutoff (updated every 10 steps), a 20.0 Å electrostatic cutoff, and a 4.0 Å hydrogen bond cutoff were used in each stage of the calculation. The minimization was performed in two stages. In the first stage, a harmonic constraint was placed on all the TMH backbone torsions (φ, ψ, and ω); this was done to preserve the general shape of the helices during minimization. In addition, the backbone atoms of the loops were frozen. The minimization consisted of a conjugate gradient minimization using a distance-dependent dielectric of 2.0, performed for 500 steps. In the second stage of the calculation, the TMH bundle was frozen, but the loops were allowed to relax. The Generalized Born/Surface Area (GB/SA) continuum solvation model for water as implemented in Macromodel was used. This stage of the calculation consisted of a Polak−Ribier conjugate gradient minimization for 500 steps. Figure 2 illustrates an extracellular view of the resultant GPR55 R model.

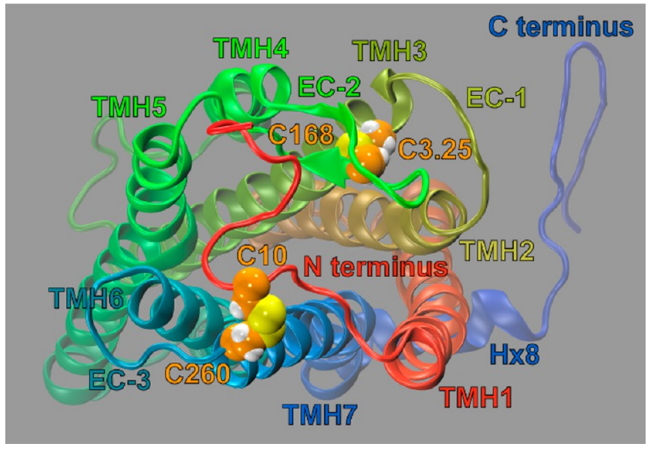

Figure 2. Extracellular view of the GPR55 inactive state (R) model. The locations of the two extracellular disulfide bridges are indicated.

Conformational Analysis of CID Compounds. Complete conformational analyses of ML191, ML192, and ML193 were performed using *ab initio* Hartree−Fock calculations at the 6-31G* level as encoded in Spartan '08 (Wavefunction, Inc., Irvine, CA). Figure 1 provides the numbering system for each compound. HF 6-31G* 6-fold conformer searches were performed for the rotatable bonds [CID23612552 (ML191) bonds, C2−C3, C3−C4, C9−N10, and C13−C14; CID1434953 (ML192) bonds, C2−N3, N6−C7, and C7−C9; and CID1261822 (ML193) bonds, C2−C3, C5−C6, N7−C8, C11−S12, S12−N13, and N13−C14]. In each conformer

dx.doi.org/10.1021/bi4008885 | *Biochemistry* 2013, 52, 9456−9469

search, local energy minima were identified by rotation of a subject torsion angle through 360° in 60° increments (6-fold search), followed by HF 6-31G* energy minimization of each rotamer generated. To calculate the energy difference between the global minimal energy conformer of each compound and its final docked conformation, rotatable bonds in the global minimal energy conformer were driven to their corresponding value in the final docked conformation and the single-point energy of the resultant structure was calculated at the HF 6-31G* level.

Electrostatic Potential Map Calculation. The electrostatic potential density surface for each ligand was calculated using Spartan '08 (Wave function, Inc.). The electrostatic potential energy was calculated using the *ab initio* Hatree−Fock method at the 6-31G* level of theory and was mapped on the 0.002 isodensity surface of each molecule. The surface was color-coded according to the potential, with electron rich regions colored red and electron poor regions colored blue.

Docking of Ligands. The lowest-energy conformation of each antagonist was manually docked in our inactive model of GPR55. The automatic docking program, Glide version 5.7 (Schrödinger Inc.), was then used to explore other possible receptor binding modes for each compound. Glide was used to generate a grid based on the centroid of select residues in the binding site (from the manual dock). The grid defines the region in which Glide is allowed to attempt to dock ligands. The grid dimensions were 26 Å × 26 Å × 26 Å; this grid size allowed Glide to thoroughly explore the receptor for possible binding sites. Other than the requirement that ligands must be docked within the grid, no constraints were used. Standard precision (SP) was selected for the docking setup. The receptor and ligand van der Waals radii were set to the default value of 0.80, and the maximal number poses to be produced was also set to 1000.

Ligand−Receptor Complex Minimization. The energies of the receptor−ligand complexes, including loop regions, were minimized using the OPLS 2005 force field in Macromodel version 9.9 (Schrödinger Inc.). Because the receptor model was minimized before the docking of the ligands, only a brief minimization was necessary to resolve any steric clashes after docking. An 8.0 Å extended nonbonded cutoff (updated every 10 steps), a 20.0 Å electrostatic cutoff, and a 4.0 Å hydrogen bond cutoff were used in each stage of the calculation. The minimization was performed in two stages. In the first stage, a harmonic constraint was placed on all the TMH backbone torsions (φ, ψ, and ω); this was done to preserve the general shape of the helices during minimization. In addition, the backbone atoms of the loops were frozen. No constraints were placed on the ligands during this stage. The minimization consisted of a conjugate gradient minimization using a distance-dependent dielectric of 2.0, performed for 500 steps. In the second stage of the calculation, the ligand and TMH bundle were frozen, but the loops were allowed to relax. The GB/SA continuum solvation model for water as implemented in Macromodel was used. This stage of the calculation consisted of a Polak−Ribier conjugate gradient minimization for 500 steps.

Interaction Energy Calculations. After the atoms of each ligand had been defined as one group (group 1) and the atoms corresponding to a residue that lines the binding site in the final ligand−GPR55 R complex had been defined as another group (group 2), Macromodel version 8.6 (Schrödinger, LLC, New York, NY) was used to output the pair interaction energy (Coulombic and van der Waals) for a given pair of atoms. The pairs corresponding to group 1 (ligand) and group 2 (residue of interest) were then summed to yield the energy of interaction between the ligand and that residue. The total of the interaction energies for all residues in the binding site was summed with the conformational cost for the ligand to assume its conformation in the final complex. This sum yielded the total interaction energy for each ligand−GPR55 R complex.

Molecular Dynamics Simulation of Ligands Docked at GPR55 R (inactive). The minimized models of the antagonist docked in GPR55 R (inactive) were further studied using molecular dynamics. The OPLS2005 force field was utilized with a distance-dependent dielectric (coefficient of 2.0 to match the docking studies). The extended nonbonded treatment was employed, as in the minimization procedure discussed above. The dynamics module of Macromodel version 9.1 was invoked, using stochastic dynamics at 300 K with the use of SHAKE constraints for bonds to hydrogen allowing a 1.5 fs time step. The models were first minimized for 500 steps with restraints on all the heavy atoms, using a large force constant of 4184 kJ/mol. The molecular dynamics was then initialized to 300 K, and an initial 100 ps of molecular dynamics was run. Subsequently, these restraints were slowly released for the side chain heavy atoms (4184−0.05 kJ/mol halving in each step for a total of 16 steps), and at each step, 150 ps of dynamics was performed. Finally, a 22.5 ns molecular dynamics simulation was conducted. Because the goal of this simulation was to explore the dynamic behavior of the antagonists in the binding pocket, in these simulations only the amino acid side chains and ligands were free to move. Visual Molecular Dynamics (VMD) was used to evaluate root-mean-square deviations (rmsds), as well interactions between the ligands and residues as a function of simulation time.

RESULTS

Identification and Biochemical Characterization of GPR55 Antagonists. ML191 (CID23612552) (5-phenyl-3-{1-[1-(*p*-tolyl)cyclopropane-carbonyl]piperidin-4-yl}-1,3,4-oxadiazol-2(3*H*)-one), ML192 (CID1434953) {furan-2-yl[4-(2-methyl-5,6,7,8-tetrahydrobenzo[4,5]thieno[2,3-*d*]pyrimidin-4-yl)piperazin-1-yl]methanone}, and ML193 (CID1261822) (*N*-{4-[*N*-(3,4-dimethylisoxazol-5-yl)sulfamoyl]phenyl}-6,8-dimethyl-2-(pyridin-2-yl)quinoline-4-carboxamide) (Figure 1) were identified in a high-throughput screen on the basis of their ability to inhibit the response of LPI to recruit a a β-arrestin-GFP reporter.[11] These ligands were chosen for computer modeling of the GPR55 binding pocket because of their potencies, IC_{50} values of 702−1076 nM, and their selectivity for GPR55 over GPR35, CB1, and CB2 in the β-arrestin translocation assay in U2OS cells permanently expressing HA-GPR55E and βarr2-GFP[11] (Figure 1). Figure 3 illustrates concentration response curves for antagonist activity in the β-arrestin trafficking assay. ML191, ML192, and ML193 inhibited trafficking induced by 10 μM LPI with IC_{50} values of 1.08 ± 0.03, 0.70 ± 0.05, and 0.22 ± 0.03 μM, respectively [mean ± standard error of the mean (SEM); $n \geq 2$] (Figure 3A). A similar rank order of antagonist potency was obtained using a different agonist, ML186 (CID15945391) [*N*-(2-methoxy-5-morpholin-4-ylsulfonylphenyl)-4,5,6,7-tetrahydro-1-benzothiophene-2-carboxamide] (Figure 3B). ML191, ML192, and ML193 inhibited trafficking induced by 1 μM ML186 with IC_{50} values of 1.03 ± 0.03, 0.29 ± 0.09, and 0.12 ± 0.02 μM, respectively (mean ± SEM; $n \geq 2$) (Figure 3B).

dx.doi.org/10.1021/bi4008885 | *Biochemistry* 2013, 52, 9456−9469

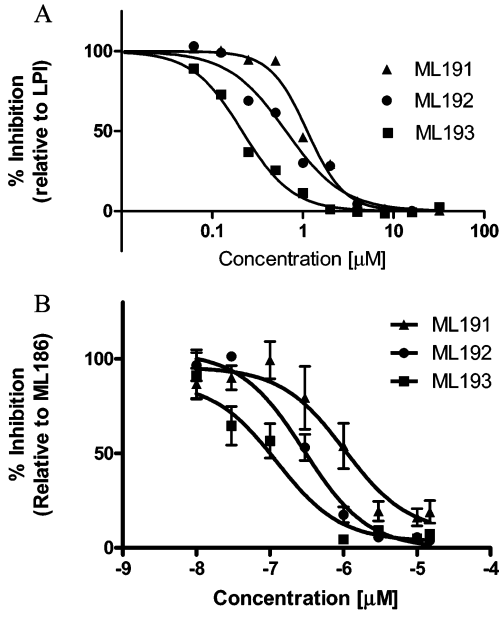

Figure 3. Antagonist activity of ML191, ML192, and ML193. Concentration response curves for the antagonist activity of ML191, ML192, and ML193 in the β-arrestin trafficking assay using LPI (A) or ML186 (B) as an agonist.

We and others have previously demonstrated the ability of LPI to activate the ERK1/2 pathway.[5,15,20] GPR55 antagonists were therefore evaluated for their ability to inhibit ERK1/2 phosphorylation in GPR55-expressing U2OS cells (Figure 4). Inhibition curves for LPI-mediated ERK1/2 phosphorylation revealed a significant decrease in the level of ERK1/2 phosphorylation and yielded IC_{50} values of 0.4 ± 0.1, 1.1 ± 0.3, and 0.2 ± 0.3 μM for ML191 (Figure 4A), ML192 (Figure 4B), and ML193 (Figure 4C), respectively. In untransfected U2OS cells, neither LPI nor any of the antagonist compounds induced ERK1/2 phosphorylation, while activation by pervanadate indicated that the MAPK pathway was intact (Figure 4D). In addition, all compounds inhibited PKCβII translocation (Table 1). This imaging assay utilizes HEK-293 cells transiently expressing a PKCβII-GFP biosensor and a wild-type GPR55 receptor.[11,21] Upon agonist treatment, the GPR55-mediated G protein signaling is measured by the recruitment of PKCβII-GFP to the plasma membrane and formation of widespread plasma membrane remodeling. This PKC recruitment is shown as increased fluorescence on the plasma membrane and development of blebs. The inhibitory effect of the probe compounds was determined by quantifying inhibition of the recruitment of PKCβII-GFP to the plasma membrane and formation of widespread plasma membrane remodeling in the presence of agonist. Because of the manual image analysis, results were binned into five categories (0, ~1, ~10, ~30, and ~60% GFP membrane recruitment and bleb formation), and compounds were tested at four concentrations (see Table 1).

Ligand Conformational Analysis. *Global Minimum Energy Conformers of GPR55 Antagonists.* Overall, the GPR55 probe molecules have three regions. The first two regions include a broad or bent head connected to a central portion of the ligand that is vertical. Together, this gives these molecular sections the shape of the number 7 (ML191 and ML192) or the letter T (ML193). The third section at the end of the vertical segment is a pendant aromatic or heterocyclic ring that is nearly perpendicular to the vertical segment (see Figure 1 for structures). At the global minimal energy conformer of CID23612552 (ML191), the *p*-methylphenyl ring is at an angle with the carbonyl group that joins the cyclopropyl and the piperidine rings (C1−C2−C3−C4 angle of 53.5° and C2−C3−C4−N6 angle of 72.5°). The piperidine, which is in a chair conformation, and the attached 1,3,4-oxadiazo-2-one ring form the vertical segment of the number 7. The 1,3,4-oxadiazo-2-one ring is perpendicular to the plane of the piperidine ring (H−C9−N10−C11 angle of −179.9°), and the pendant phenyl ring is in plane with the 1,3,4-oxadiazo-2-one ring (O12−C13−C14−C15 angle of −0.4°).

At the global minimal energy conformer of CID1434953 (ML192), the molecule has the piperazine ring (part of the vertical segment of the number 7) out of plane with the thienopyrimidine group (N1−C2−N3−LP angle of 137.1°). The piperazine is in a chair conformation, and the N3 lone pair points 180° away from the N6 lone pair. The lone pair of the piperazine N6 atom is almost perpendicular to the carbonyl group (O8−C7−N6−LP angle of −115.3°) that connects the piperazine to the furan ring. The pendant furan ring is nearly in plane with the carbonyl group (O8−C7−C9−C10 angle of −2.0°).

The global minimal energy conformer of CID12440433 (ML193) has the pyridine ring almost coplanar to the dimethylquinoline ring (N1−C2−C3−C4 angle of 3.7°). The amide group is out of plane with the dimethylquinoline ring (C4−C5−C6−N7 angle of −48.5°) and nearly in plane with the central phenyl ring (C6−N7−C8−C9 angle of −5.8°). The sulfonamide group is perpendicular to the central phenyl ring (C10−C11−S12−N13 angle of 89.2°), and the nitrogen of the sulfonamide is cupped with the nitrogen lone pair pointing down, in the opposite side of the rest of the molecule (C11−S12−N13−LP angle of −173.5°). The plane of the pendant dimethylisoxazole ring is almost perpendicular to the axis formed by the N−S bond of the sulfonamide (S12−N13−C14−O15 angle of −103.1°). The methyl groups of the dimethyloxazole are pointing down, away from the rest of the molecule.

GPR55 Agonist Molecular Electrostatic Potential Maps. Figure 5 illustrates the molecular electrostatic potential maps (ranges in kilojoules per mole given next to each ligand) of the docked conformations of ML191, ML192, and ML193 at GPR55 R. In the second row, the conformer of each used to calculate the map is shown in tube display. Each ligand possesses a head region connected to a central portion of the ligand that has a thin profile. The most electronegative region of each ligand is located close to the far end of this central section, and this portion is followed by a pendant aromatic or heterocyclic ring that juts out nearly perpendicular to the central portion of the molecule. The carbonyl oxygen of the 1,3,4-oxadiazo-2-one ring of ML191, the amide group carbonyl oxygen of ML192, and the sulfonamide oxygens of ML193 are the most or some of the most electronegative regions of the ligands and form the part of each molecule that interacts with K2.60(80) (see docking results below).

GPR55 Inactive (R) State Model. Because ML191, ML192, and ML193 are GPR55 antagonists, each was docked in the inactive state model of GPR55. In this model, there is a hydrogen bond between R3.50(119) and Q6.30(221) that corresponds to the R3.50-D/E6.30 "ionic lock" found in many class A GPCRs. This hydrogen bond is facilitated by the SFLP hinge motif (CWXP in most class A receptors) that hinges the

dx.doi.org/10.1021/bi4008885 | *Biochemistry* 2013, 52, 9456−9469

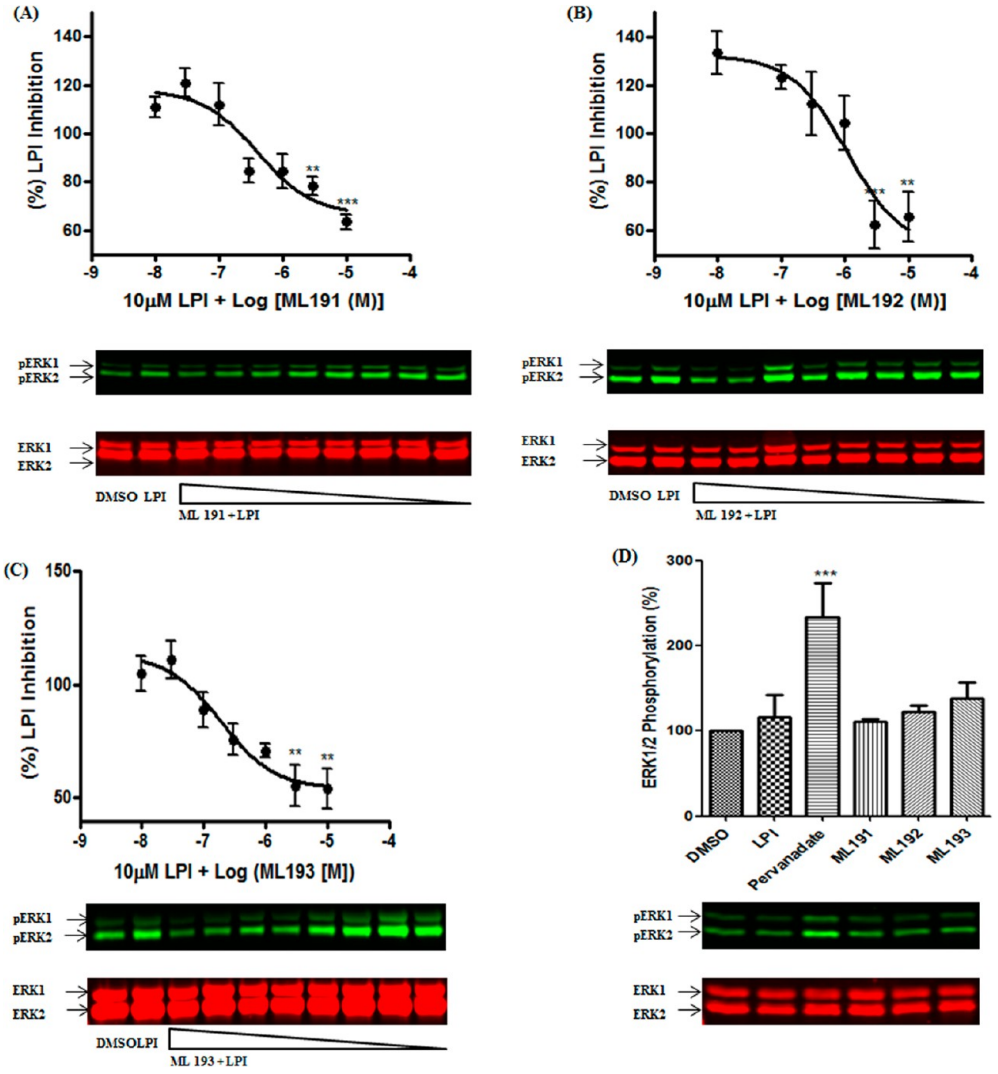

Figure 4. LPI-mediated ERK1/2 phosphorylation is largely inhibited by ML191, ML192, and ML193 in U2OS cells overexpressing GPR55E and βarr2-GFP. Cells were preincubated with increasing concentrations of ML compounds 30 min prior to the application of LPI (10 μM). ERK1/2 phosphorylation levels were monitored and normalized to total ERK1/2 levels, and the IC_{50} value for each of the compounds was determined. Data are means ± SEM from three independent experiments performed in duplicate (*P < 0.05, **P < 0.01, and ***P < 0.001). LPI-mediated ERK1/2 phosphorylation was significantly attenuated following treatment with ML191 (A), ML192 (B), and ML193 (C). In untransfected U2OS cells, neither LPI nor any of the antagonist compounds induced ERK1/2 phosphorylation, while activation by pervanadate indicated that the MAPK pathway is intact (D).

Table 1. Inhibition of PKCβII Translocation (AID 488947) in Cells with the Wild-Type GPR55 Receptor[a]

	membrane recruitment/Bleb formation			
	100 μM	30 μM	10 μM	0 μM
ML191	−	+	++	++++
ML192	+	+++	++++	++++
ML193	−	−	+	++++

[a]Manual image analysis result definition: −, no GFP membrane recruitment or bleb formation; +, ∼1% GFP membrane recruitment or bleb formation; ++, ∼10% GFP membrane recruitment or bleb formation; +++, ∼30% GFP membrane recruitment or bleb formation; ++++, ∼60% GFP membrane recruitment or bleb formation.

intracellular end of TMH6 toward the intracellular end of TMH3. The interaction of these two residues closes the intracellular side of the receptor to any interaction with G protein. Within the binding pocket of each class A GPCR is a set of residues for which agonist binding promotes a conformational change. For many class A GPCRs, these "toggle switch" residues include a residue on TMH6 close to the TMH6 CWXP motif and a residue (or covalently bound ligand) that interacts directly with this TMH6 residue. In rhodopsin, W6.48 (part of the TMH6 CWXP hinge motif) adopts a g^+ χ^1 dihedral angle. In the inactive state of rhodopsin, 11-*cis*-retinal's β-ionone ring directly interacts with W6.48, blocking its movement.[22−24] When rhodopsin is light activated, 11-*cis*-retinal isomerizes to all-*trans*-retinal and the β-ionone ring moves away from TMH6 and toward TMH4.[37] This movement frees the χ^1 of W6.48 to undergo a $g^+ \rightarrow$ *trans* conformational change.[25] Mutational studies have shown that W6.48 and F3.36 form the toggle switch in the cannabinoid CB1 receptor.[26] In the crystal structure of the agonist-bound β_2-adrenergic receptor, the residues that comprise the toggle switch are F6.44, P5.50, and I3.40.[27] When agonist binding trips the toggle switch within the binding pocket, TMH6 becomes straighter (using the CWXP hinge motif) and moves

dx.doi.org/10.1021/bi4008885 | *Biochemistry* 2013, 52, 9456−9469

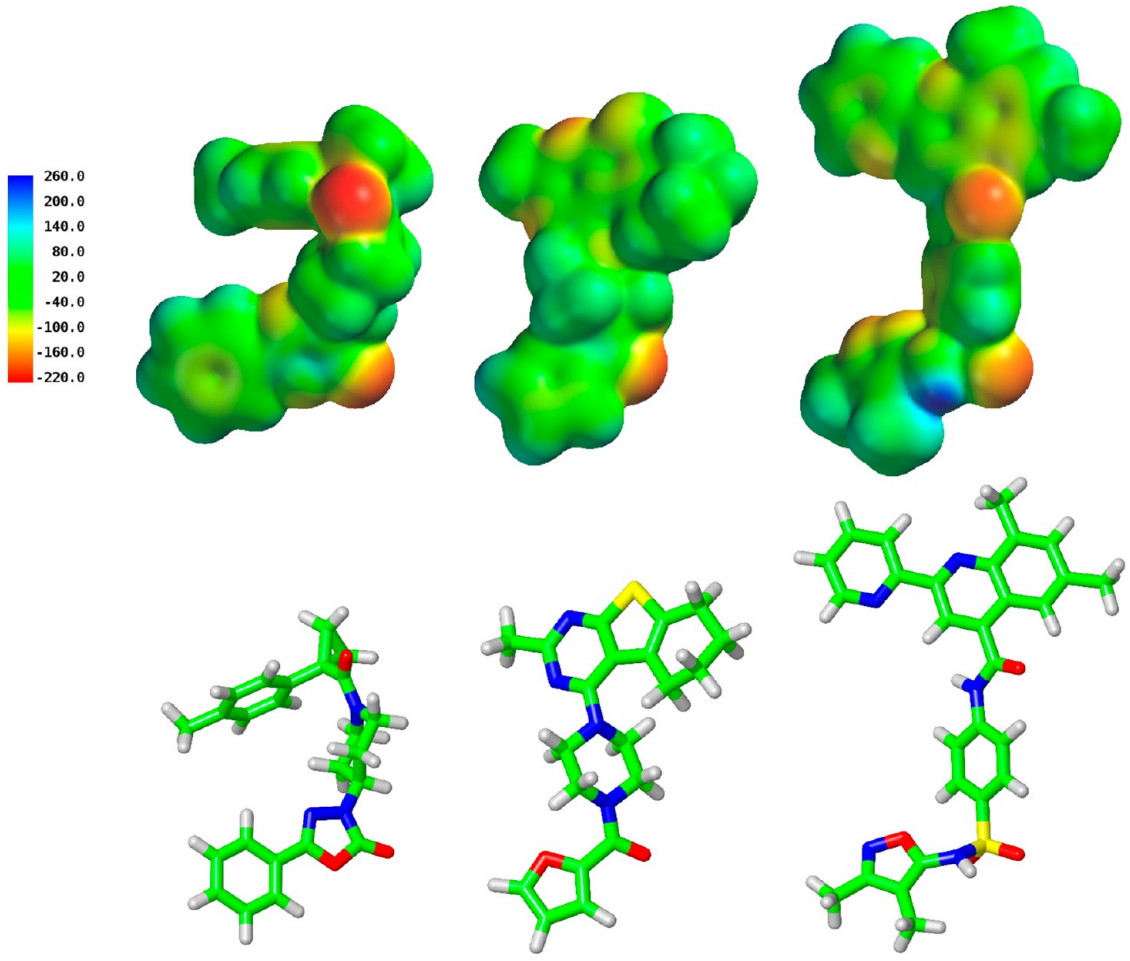

Figure 5. Molecular electrostatic potential maps of ML191, ML192, and ML193 (top row). Conformer of each used to calculate the map shown in tube display (bottom row).

its intracellular end away from the TMH bundle. This movement of TMH6 breaks the ionic lock between R3.50 and E/D6.30 at the intracellular end of the receptor. What results is an intracellular opening in the TMH3−TMH4−TMH5−TMH6 region large enough to allow the G-α protein to insert its α5 helix C-terminal region into the activated GPCR.[28] This sequence of events is consistent with the recent X-ray crystal structure of the β_2-adrenergic receptor in complex with Gs protein.[29]

In this paper, we are studying molecules that should prevent GPR55 from being activated. In GPR55, the TMH6 hinge motif sequence is SFLP. In the inactive state model, the χ^1 dihedral angle of F6.48(239) is g^+ and is held in this conformation by M3.36(104) (χ^1 is *trans*). We have hypothesized that the M3.36−F6.48 interaction constitutes the toggle switch for GPR55. As discussed below, one key feature of each of the GPR55 antagonists studied here is a structural component that prevents this M3.36−F6.48 toggle switch from changing conformation.

Compound Docking in the GPR55 Inactive State (R) Model. Docking studies identified the putative binding sites for ML191, ML192, and ML193 to be the TMH2−TMH3−TMH5−TMH6−TMH7 region of the GPR55 R model. Although Glide docking studies were performed without a primary interaction specified, in each case K2.60(80), the only positively charged TMH residue in the putative binding site, formed a hydrogen bond with each ligand in the final complex identified by Glide. Because ML191, ML192, and ML193 differ in size, we begin this section considering the binding pocket for ligands on the basis of size (ML193 > ML191 > ML192).

Figure 6 illustrates the ML193−GPR55 R complex obtained using Glide. The ML193 sulfonamide oxygen forms a hydrogen bond with K2.60(80). The hydrogen bond (N−O) distance and (N−H−O) angle are 2.78 Å and 178°, respectively. ML193 also forms extensive $\pi-\pi$ stacking interactions with the receptor. The N-terminal amino acid F12 stacks with the dimethylquinoline ring that forms part of the broad head region. The ring centroid−centroid distances of F12 to the fused dimethylbenzyl and pyridyl rings of the dimethylquinoline are 5.23 and 6.36 Å and angles between ring planes 93° and 91°, respectively. The EC-2 loop residue F169 forms aromatic stacking interactions with both the dimethylquinoline and the pendant pyridine rings. The ring centroid−centroid distances are 4.97 and 4.90 Å for the dimethylbenzyl and pyridyl rings of the dimethylquinoline, respectively, and 6.50 Å for the pendant pyridine ring. The angles between the ring planes are 54° for the dimethylquinoline rings and 53° for the pendant pyridine. Finally, transmembrane residue F5.39(182) forms an offset parallel stack with the pendant pyridine ring (ring centroid−centroid distance of 5.86 Å and angle between ring planes of 36°), and F6.55(246) forms a T-stack with the pendant dimethylisoxazole ring (ring centroid−centroid distance of 5.64 Å and angle between ring planes of 117°). The net Glide score for ML193 with GPR55 is −3.18 kcal/mol (see Table S.9 of the

dx.doi.org/10.1021/bi4008885 | *Biochemistry* 2013, 52, 9456−9469

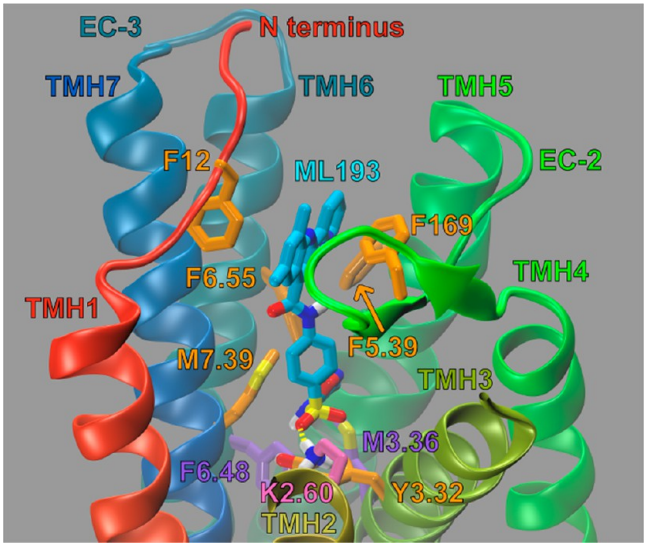

Figure 6. ML193 (blue) docked in the GPR55 R model. In the view shown here, the top of TMH7 has been omitted for the sake of clarity. K2.60(80) (pink) was observed to be a primary interaction site during docking studies. The toggle switch residues M3.36(104) and F6.48(239) are colored purple. Residues that contributed at least 2.5% to the total interaction energy are colored orange. See Table S.1 of the Supporting Information for a breakdown of the energy of interaction of ML193 in GPR55 R with specific residues.

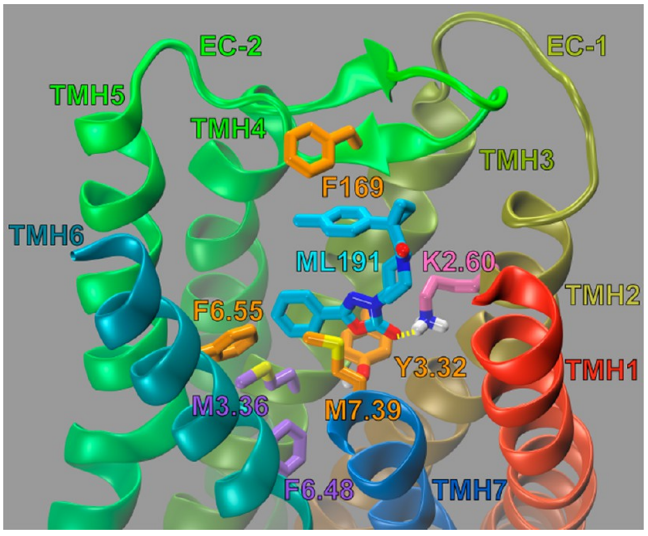

Figure 7. ML191 (blue) docked in the GPR55 R model. In the view shown here, the top of TMH7 has been omitted for the sake of clarity. K2.60(80) (pink) was observed to be a primary interaction site during docking studies. Toggle switch residues M3.36(104) and F6.48(239) are colored purple. Residues that contributed at least 2.5% to the total interaction energy are colored orange. See Table S.2 of the Supporting Information for a breakdown of the energy of interaction of ML191 in GPR55 R broken down by residue.

Supporting Information). The hydrogen bonding interaction with K2.60(80) and the van der Waals interactions with M7.39(274) are the major contributors to the interaction energy. The aromatic stacking interactions with F169, Y3.32(101), and F12 add significantly to the interaction energy. Finally, Q7.36(271), Q6.58(249), and F3.33(102) contribute some van der Waals interaction energy for the complex. The pendant dimethylisoxazole ring prevents a change in the χ^1 of M3.36(104) and therefore keeps GPR55 in the inactive state. The interaction energy for ML193 with specific GPR55 binding pocket residues is summarized in Table S.1 of the Supporting Information. The conformational energy cost for ML193 to adopt the docked conformation is 2.34 kcal/mol, and the rmsd between the docked conformation and the global minimum energy conformer is 2.14 (see Table S.10 of the Supporting Information).

Figure 7 illustrates the ML191−GPR55 R complex obtained using Glide. The ML191 1,3,4-oxadiazo-2-one carbonyl oxygen forms a hydrogen bond with K2.60(80). The hydrogen bond distance (N−O) and angle (N−H−O) are 2.81 Å and 166°, respectively. ML191 forms a number of aromatic stacking interactions. The methylphenyl ring next to the cyclopropyl group forms a stack with the EC-2 loop residue F169 (ring centroid−centroid distance of 5.27 Å and angle between ring planes of 117°). The pendant phenyl group adjacent to the 1,3,4-oxadiazo-2-one ring stacks with F6.55(246). The ring centroid−centroid distance is 5.71 Å, and the angle between ring planes is 60°. The net Glide score for ML191 with GPR55 is −2.25 kcal/mol (see Table S.9 of the Supporting Information). The major interaction energy contributions for this compound are the hydrogen bonding interaction with K2.60(80) and van der Waals interactions with M7.39(274). Aromatic stacking interactions with F169 and van der Waals interactions with Y3.32(101) also contribute to the interaction energy. The remainder of the aromatic stacking interactions identified contribute less to the overall interaction energy. The pendant phenyl group prevents a change in the χ^1 of the toggle switch residue, M3.36(104), and therefore keeps GPR55 in the inactive state. The interaction energy for ML191 with specific residues is summarized in Table S.2 of the Supporting Information. The conformational energy cost for ML191 to adopt the docked conformation is 2.09 kcal/mol, and the rmsd between the docked conformation and the global minimal energy conformer is 0.71 (see Table S.10 of the Supporting Information).

Figure 8 illustrates the ML192−GPR55 R complex obtained using Glide. The ML192 carbonyl oxygen preceding the pendant furan ring hydrogen bonds with K2.60(80). The hydrogen bond distance (N−O) and angle (N−H−O) are 2.79 Å and 160°, respectively. Additionally, two phenylalanines form aromatic stacking interactions with the ligand. The EC-2 loop residue F169 stacks with the aromatic rings of the fused ring system in the broad head region of the molecule. The ring centroid−centroid distances from F169 to the pyrimidine and thiophene rings are 5.77 and 5.21 Å, respectively, and the angles between the ring planes are 73° and 73°, respectively. Transmembrane residue F3.33(102) forms an aromatic T-stack with the pendant furan ring that juts out nearly perpendicular to the central portion of the molecule (distance of 4.58 Å and angle of 35°). The net Glide score for ML192 with GPR55 is −1.23 kcal/mol (see Table S.9 of the Supporting Information). While the hydrogen bonding interactions with K2.60(80) and the aromatic stacking interaction with F169 contribute to the interaction energy, van der Waals interactions with the hydrophobic residue M7.39(274) make a major contribution to the total interaction energy of this complex. Finally, amino acids E3.29(98), Y3.32(101), F12, Q7.36(271), and S7.32(267) make smaller van der Waals contributions to the interaction energy. ML192 is significantly smaller than ML193 and ML191 and therefore does not penetrate the binding pocket as deeply. ML192 interacts directly with F3.33(102), which in turn

dx.doi.org/10.1021/bi4008885 | *Biochemistry* 2013, 52, 9456−9469

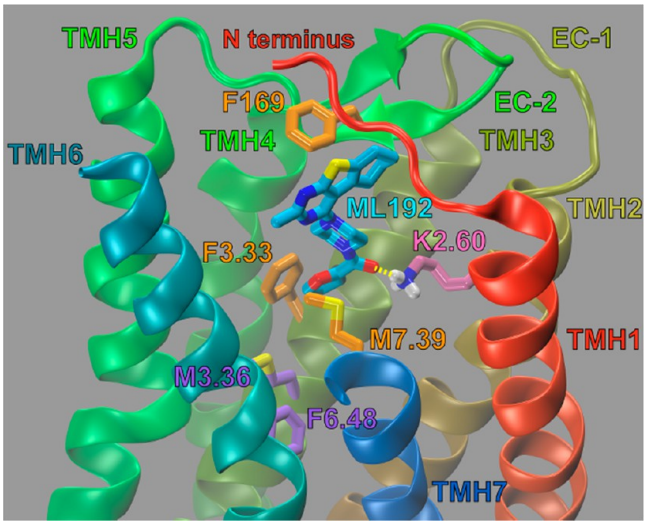

Figure 8. ML192 (blue) docked in the GPR55 R model. In the view shown here, the top of TMH7 has been omitted for the sake of clarity. K2.60(80) (pink) was observed to be a primary interaction site during docking studies. Toggle switch residues M3.36(104) and F6.48(239) are colored purple. Residues that contributed at least 2.5% to the total interaction energy are colored orange. See Table S.3 of the Supporting Information for a breakdown of the energy of interaction of ML192 in GPR55 R broken down by residue.

interacts with the toggle switch residue, M3.36(105). This interaction would prevent the movement of M3.36(105), and therefore, ML192 keeps GPR55 in the inactive state. The interaction energy for ML192 with specific residues is summarized in Table S.4 of the Supporting Information. The conformational energy cost for ML192 to adopt the docked conformation is 3.51 kcal/mol, and the rmsd between the docked conformation and the global minimal energy conformer is 0.25 (see Table S.10 of the Supporting Information).

Correlation of Interaction Energies with Biological Results. It is interesting to note that GPR55 R net Glide energies (Table S.9 of the Supporting Information) calculated for the three antagonists reported here [ML193 (−3.18 kcal/mol) < ML191 (−2.25 kcal/mol) < ML192 (−1.23 kcal/mol)] correlate best with the trend in potency in the PKCβII translocation assay, with ML-193 being the most potent antagonist and also the ligand with the highest net Glide score. In the β-arrestin trafficking assay (vs LPI and ML186) and in the LPI- mediated ERK1/2 phosphorylation assay, ML193 remains the most potent antagonist; however, ML192 ranks as the next most potent antagonist in these assays.

Molecular Dynamics Simulation of Antagonist−Receptor Complexes. To elucidate the dynamic behavior of ML191, ML192, and ML193 with the receptor, a 22.5 ns molecular dynamics simulation was run on the final three antagonist−GPR55 complexes (shown in Figures 6, 7, and 8). Specifically, the simulations were run for three reasons: (1) to observe if the general binding site (that was proposed in the static models) for each antagonist persists or if it evolves over the simulation trajectory, (2) to observe if the interaction (as proposed in the static model) between each antagonist and K2.60(80) persists in a dynamic simulation, and (3) to observe if the interaction between each antagonist and M3.36(104) [either directly or via F3.33(102)] persists in a dynamic simulation.

The ML193−GPR55 complex did not significantly change over the course of the simulation trajectory. Specifically, Figure S.1 of the Supporting Information illustrates that the rmsd for the receptor is quite low and does not significantly change over the course of the simulation. In addition, Figure S.2 of the Supporting Information illustrates that ML193's rmsd was low and did not significantly change over the course of the trajectory, with the exception of an increase from 16 to 18 ns, which was followed by a return to the previous rmsd value for the rest of the simulation. This change in rmsd between 16 and 18 ns is caused by the pyridine ring flipping 180° and then returning to its original position. This is captured by the ω^1 torsion angle (see Figure S.4 of the Supporting Information for the structure and Figure S.3 of the Supporting Information for the dihedral plot). ML193 maintained a hydrogen bond with K2.60(80) for 58.2% of the trajectory but stays in the proximity of K2.60(80) throughout the simulation. ML193 also forms a hydrogen bond between the amide oxygen and Q7.36(271) for 6.4% of the trajectory (see Table S.11 of the Supporting Information). Together, these results are consistent with the binding mode for ML193 proposed by the static model.

The ML191−GPR55 complex also did not significantly change over the course of the simulation trajectory. Specifically, Figure S.5 of the Supporting Information illustrates that the rmsd for the receptor is quite low and does not significantly change over the course of the simulation. Figure S.6 of the Supporting Information illustrates that the rmsd for ML191 is low with the exception of the periods between 4 and 6 ns and between 20 and 22.5 ns. During these two time periods, the phenyl ring rotates from 180° to 0°. This is captured by the ω^5 torsion angle (see Figure S.8 of the Supporting Information for the structure and Figure S.7 of the Supporting Information for the dihedral plot). ML191 maintained a hydrogen bond with K2.60(80) for 93.1% of the trajectory (see Table S.11 of the Supporting Information). These results suggest that the proposed static model of the ML191−GPR55 complex is stable and that ML191's location and interactions with the receptor do not significantly change during the simulation.

ML192 is the smallest of the three GPR55 antagonists considered here and the antagonist with the poorest net Glide score (−1.23 kcal/mol). MD simulations showed this ligand to be more mobile in the binding pocket. This is reflected in an increased rmsd for the ligand (see Figure S.10 of the Supporting Information) relative to ML193 and ML191. However, the conformation of receptor does not significantly change; this can be observed by the low rmsd for the receptor (see Figure S.9 of the Supporting Information). Figure S.11 of the Supporting Information illustrates that ML192's dihedral angles (see Figure S.12 of the Supporting Information for dihedral definitions) have persistent values throughout the simulation except during the period from 3 to 5 ns. This is captured by the ω^3 torsion angle (see Figure S.12 of the Supporting Information), which changes from 60° to −60° at 3 ns but switches back at 5 ns and then stays 60° for the remainder of the simulation. ML192 maintains its interaction with K2.60(80), as predicted by the static model. ML192 forms a hydrogen bond with K2.60(80) for 44.2% of the simulation. In addition, ML192 formed a hydrogen bond with Q7.36(271) and S7.32(267) for a significant duration of the simulation [35.3 and 27.9% of the simulation, respectively (see Table S.11 of the Supporting Information)].

MD studies suggested that ML192 was mobile enough to adopt a binding region more extracellular than that of the static ML192−GPR55 R dock. To understand the differences, we extracted the last frame from the MD trajectory and energy-

dx.doi.org/10.1021/bi4008885 | *Biochemistry* 2013, 52, 9456−9469

minimized the system using the same minimization protocol as described above. Figure 9 illustrates the ML192−GPR55 R complex obtained from this frame of the molecular dynamics simulation. The ML192 carbonyl oxygen preceding the pendant furan ring hydrogen bonds with K2.60(80). The hydrogen bond distance (N−O) and angle (N−H−O) are 3.12 Å and 130°, respectively. Interestingly, K2.60(80) also forms a hydrogen bond with Q7.36(271); the hydrogen bond distance (N−O) and angle (N−H−O) are 2.83 Å and 167°, respectively. In turn, Q7.36(271) forms a hydrogen bond with one of ML192's pyrimidine nitrogens; the hydrogen bond distance (N−N) and angle (N−H−N) are 3.10 Å and 162°, respectively. Additionally, two phenylalanines form aromatic stacking interactions with the ligand. The N-terminal residue F12 stacks with the aromatic rings of the fused ring system in the broad head region of the molecule. The ring centroid−centroid distances from F12 to the pyrimidine and thiophene rings are 5.10 and 4.88 Å, respectively, and the angles between the ring planes are both 61°. The EC-2 loop residue F169 also stacks with the aromatic rings of the fused ring system in the broad head region of the molecule. The ring centroid−centroid distances from F169 to the pyrimidine and thiophene rings are 5.68 and 4.82 Å, respectively, and the angles between the ring planes are 134° and 133°, respectively. The net Glide score for this MD frame was poor (−0.16 kcal/mol). It is interesting, however, that even though ML192 is higher in the binding pocket here, it still would function as an antagonist because it would inhibit the movement of the EC-2 loop (see Discussion).

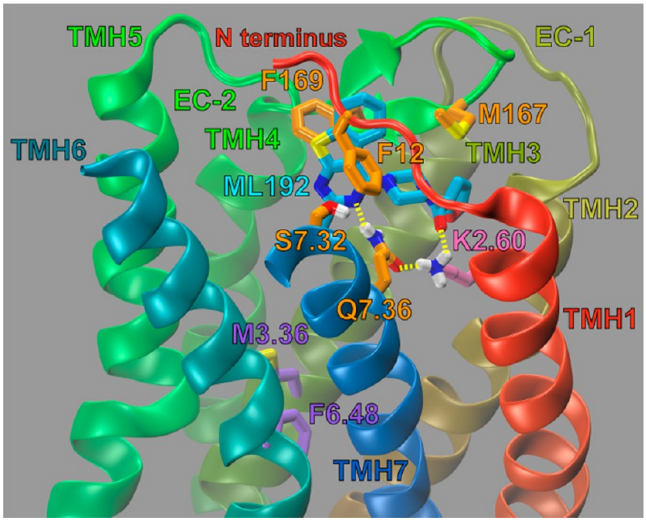

Figure 9. MD studies suggested that ML192 was more mobile in the binding pocket such that it could adopt a binding region more extracellular than that of the static ML192−GPR55 R complex. To understand the differences, we extracted a frame from the MD trajectory and energy-minimized the system using the same minimization protocol described above. The results are illustrated here. ML192 (blue) is shown docked in the GPR55 R model. In the view shown here, the top of TMH7 has been omitted for the sake of clarity. K2.60(80) (pink) was observed to be a primary interaction site during the molecular dynamics simulation. Toggle switch residues M3.36(104) and F6.48(239) are colored purple. Residues that contributed at least 2.5% to the total interaction energy are colored orange. See Table S.4 of the Supporting Information for a breakdown of the energy of interaction of ML192 in GPR55 R broken down by residue.

DISCUSSION

High-throughput screening has revolutionized our ability to identify new chemotypes acting at GPCRs. This has been particularly true for the GPR55 field because the initial use of cannabinoid receptor/lipid-biased compound libraries led to a low level of chemical diversity and a lack of receptor selectivity. On the basis of the docking and MD studies reported here, we propose that each of the antagonists (ML191, ML192, and ML193), although they are from very different chemotypes, share important conformational and electronic features that result in similar binding modes and antagonism of GPR55. These GPR55 antagonists possess (1) a head region that occupies a horizontal binding pocket near the extracellular (EC) end of GPR55, (2) a central ligand portion that fits vertically in the receptor binding pocket with the most electronegative region of each ligand located close to the far end of this central section, and (3) a pendant aromatic or heterocyclic ring that juts out from the central section and is located deepest in the binding pocket. The pendant aromatic or heterocyclic ring binds deep enough in the binding pocket to block M3.36(104) [or a residue that blocks M3.36(104)], preventing the M3.36(104)−F6.48(239) toggle switch from undergoing the conformational change that is likely associated with GPR55 activation. However, because the primary interaction site for the most electronegative region of each ligand is K2.60(80), which is located only two turns down from extracellular loops, a portion of each of these antagonists extends into the EC loop region of GPR55. The fact that these ligands also extend into EC receptor regions may be an additional feature important for their function as antagonists.

GPCR Activation. Antagonists block receptor activation. It is therefore important to understand how these receptors are activated. While there are likely multiple activated states of a given receptor depending on the agonist that triggers activation, there are commonalities among all of these activated states both in the intracellular domains and within the binding pocket.

Intracellular Domain. The structural characteristics that define the GPCR inactive (R) and active (R*) states have been deduced primarily from biophysical studies of rhodopsin and the β_2-AR. In the inactive or off state (R), the intracellular (IC) end of TMH6 is bent toward TMH3 and a salt bridge between R3.50 and E/D6.30 on the intracellular side of the TMH bundle forms an ionic lock. In the activated state, TMH6 undergoes a conformational change, becoming straighter in the highly conserved CWXP hinge region.[30−35] This results in the intracellular ionic lock breaking as TMH3 and TMH6 move away from each other.[36] The intracellular opening created by this change allows the G protein then to couple to the receptor. In our model of the GPR55 inactive state, the intracellular ends of TMH3 and TMH6 are kept in the proximity of each other by a hydrogen bond between R3.50(119) and Q6.30(221) that functions as GPR55's ionic lock.

Binding Pocket. The change from the inactive to active state also is associated with changes within the ligand binding pocket. In the R state, a tryptophan residue in the CWXP hinge motif on TMH6, W6.48, adopts a g^+ χ^1 dihedral angle. This conformation in rhodopsin is due to the proximity of the β-ionone ring of rhodopsin's covalently bound ligand, 11-*cis*-retinal, to W6.48, such that the tryptophan is locked in place.[22−24] W6.48 is part of the highly conserved TMH6 CWXP motif and has been identified as being important for GPCR activation through early mutagenesis studies. An X-ray

dx.doi.org/10.1021/bi4008885 | *Biochemistry* 2013, 52, 9456−9469

crystal structure of a constitutively active rhodopsin mutant suggests that when rhodopsin is activated and undergoes the isomerization from 11-*cis*-retinal to all-*trans*-retinal, the retinal β-ionone ring is shifted 4.3 Å toward the cleft between TMH5 and TMH6 and W6.48 is released from its locked position. The indole group of W6.48 moves 3.6 Å away from its ground state position as a consequence of rhodopsin activation,[37] and W6.48 undergoes a change in its χ^1 angle from g^+ to *trans*.[25] For the CB1 receptor, we have documented via mutation the existence of a binding pocket toggle switch that involves F3.36 and W6.48.[26,38] Here, the χ^1 of F3.36 must undergo a *trans* to g^+ conformational change to free the W6.48 χ^1 to undergo its g^+ to *trans* conformational change. In GPR55, M3.36(104) appears to serve a similar function in holding F6.48(239) in a g^+ χ^1 conformation. Although this W6.48 g^+ to *trans* conformation change in χ^1 is not seen in recent activated GPCR crystal structures, it is possible that such a change is transient and therefore not captured in the crystalline state. In fact, in molecular dynamics simulations of activation of the cannabinoid CB2 receptor by its endogenous ligand, we observed such a transient change in W6.48.[39] Likewise, a rotameric change of W6.48 has been documented to occur in microsecond long molecular dynamics simulations[40] of the β_2-adrenergic receptor in complex with Gs protein.[29]

Extracellular Regions. We show here that the GPR55 antagonist ligands, ML191, ML192, and ML193, all bind high enough in GPR55 to interact directly with and block movement of the EC-2 loop. In addition, ML192 may be mobile enough to move closer to this region while maintaining its interaction with K2.60. Extracellular loop conformational changes have been shown to be critical for signal transduction of many class A GPCRs. For example, the results of NMR studies have suggested that upon activation, rhodopsin's EC-2 loop undergoes a necessary conformational change that is coupled to the breaking of the intracellular ionic lock (i.e., an ionic interaction between R3.50 and D/E6.30 that promotes an inactive GPCR conformation).[41] Additionally, the results of recent mutational studies of the angiotensin II type 1 receptor suggest that the EC-2 loop undergoes ligand-specific conformational changes that are required for receptor activation.[42,43] Circular dichroism and steady state fluorescence studies have been used to illustrate that the EC-2 loop, of the serotonin 5-$HT_{4(a)}$ receptor, adopts specific loop conformations that are determined by the receptor's activation state.[44] Mutational studies of the cannabinoid CB1 receptor have suggested that the EC-2 loop may move down toward the transmembrane core upon receptor activation.[45,46] Thus, ligands located high enough in the binding pocket to interfere with such movements could act as antagonists by blocking these changes.

Comparisons with Other Published GPR55 Antagonists. Recently, several papers have presented other GPR55 antagonists that come from additional chemotypes. In some cases, the antagonists are selective for GPR55,[47,48] while in other cases, the ligand retains activity at one or more additional receptors.[3,49] Kargl and co-workers used CID16020046, 4-[4-(3-hydroxyphenyl)-3-(4-methylphenyl)-6-oxo-1*H*,4*H*,5*H*,6*H*-pyrrolo[3,4-*c*]pyrazol-5-yl]benzoic acid (see Figure 1 for the structure), to show that in yeast cells expressing human GPR55, CID16020046 antagonized agonist-induced receptor activation with an IC_{50} of 0.15 μM.[48] In HEK-293 cells stably expressing human GPR55 (HEK-GPR55), the compound behaved as an antagonist on LPI-mediated Ca^{2+} release and extracellular signal-regulated kinase (ERK1/2) activation, but not in HEK-293 cells expressing CB1 or CB2.[48] The dock of the *S* enantiomer of CID16020046 in GPR55 R is shown in Figure S.13 of the Supporting Information, and its interaction energies are listed in Table S.5 of the Supporting Information. Here the methylphenyl ring penetrates deepest into the binding site and prevents M3.36(104) from undergoing a conformational change. The 6-oxo group of the central heterocyclic ring has the highest electrostatic potential and hydrogen bonds with K2.60(80). The net Glide score for CID16020046 (*S* enantiomer) is −3.75 kcal/mol (see Table S.9 of the Supporting Information), and the rmsd of the docked conformation is 1.35.

The cannabis constituent, cannabidiol (CBD), has been reported to function as a GPR55 antagonist by attenuating the effects produced by GPR55 agonists O-1602 and LPI on mouse and human osteoclast polarization and resorption *in vitro*.[3] CBD has also been reported to be a low-efficacy agonist at GPR18.[50] Figure S.14 of the Supporting Information shows CBD docked in GPR55 R. Here, the pentyl side chain of CBD penetrates deepest in the binding pocket and blocks the movement of M3.36(104). The two hydroxyls of CBD interact with K2.60(80) and E3.29(99). These two interactions are the major interactions for CBD at GPR55 (see Table S.6 of the Supporting Information). The net Glide score for this complex is −2.39 kcal/mol (see Table S.9 of the Supporting Information), and the rmsd for the docked conformation relative to the global minimum is 0.64.

Docks of two other recently reported GPR55 antagonists, 3-(2-hydroxybenzyl)-5-isopropyl-8-methyl-2*H*-chromen-2-one[47] [termed Compound 12 in ref 47 (see Figure S.15 of the Supporting Information)] and tetrahydromagnolol[49] (see Figure S.16 of the Supporting Information), are included in the Supporting Information along with their interaction energies (Tables S.7 and S.8 of the Supporting Information). The net Glide score for the 3-(2-hydroxybenzyl)-5-isopropyl-8-methyl-2*H*-chromen-2-one−GPR55 R complex is −0.59 kcal/mol (see Table S.9 of the Supporting Information), and the rmsd for the docked conformation relative to the global minimum is 1.66 (see Table S.10 of the Supporting Information). The net Glide score for the tetrahydromagnolol−GPR55 R complex is −1.34 kcal/mol (see Table S.9 of the Supporting Information), and the rmsd for the docked conformation relative to the global minimum is 0.75 (see Table S.10 of the Supporting Information).

Of the four GPR55 antagonists discussed in this section, CID16020046[48] and 3-(2-hydroxybenzyl)-5-isopropyl-8-methyl-2*H*-chromen-2-one[47] are GPR55 selective, while CBD[3,50] and tetrahydromagnolol[49] act at additional receptors. It is worth noting that although CBD and tetrahydromagnolol can dock at GPR55 and function as antagonists, neither ligand conforms completely to the description of the general shape we use in this work to describe ML191, ML192, and ML193. The fact that these are also the only two ligands that lack GPR55 selectivity leads to the speculation that this shape difference may be the origin of their nonselectivity.

The Key Molecular Features That Discriminate GPR55 Agonists from Antagonists. Previously, by modeling of the GPR55 activated state, we compared the GPR55 binding conformations of three novel agonists, CID1792197, CID1172084, and CID2440433 (PubChem IDs), with that of the endogenous GPR55 agonist, LPI.[17] Our modeling indicated that the molecular shapes and electrostatic potential distributions of these agonists mimic those of LPI. We found that the

GPR55 R* binding site accommodates agonists that have T or inverted-L shapes with long, thin profiles that can fit vertically deep in the receptor binding pocket, while their broad head regions occupy a horizontal binding pocket near the extracellular end of the GPR55 TMH bundle. The most electronegative region of each agonist was located at one end of the broad head region. The structure of one of these agonists, CID1792197, is provided in Figure 10, where it is compared to the structure of the antagonist, ML191.

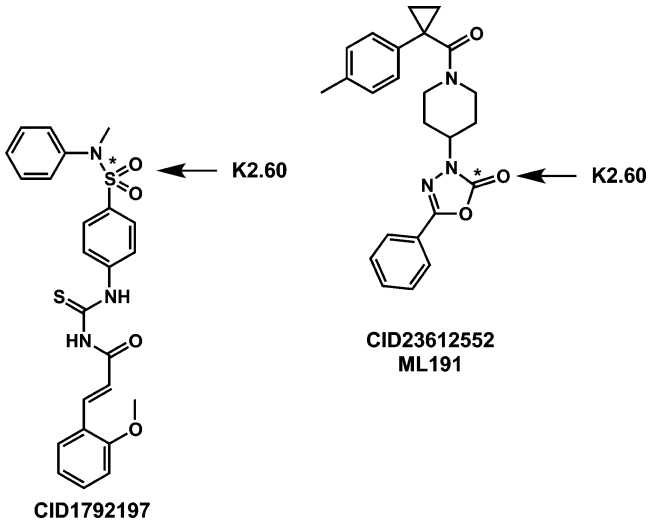

Figure 10. Structures of a GPR55 agonist (CID1792197)[17] and GPR55 antagonist (ML191). The agonist has its most electronegative region (which hydrogen bonds to K2.60) near the broad head region, while this region is found in antagonists near the end of the central portion of the molecule. In addition, agonist structures lack the pendant phenyl ring found in ML191 after the central portion. Instead, agonist structures maintain a thin vertical profile in the binding pocket.

There are two striking differences between the GPR55 agonist and antagonist structures (see Figure 10). First, GPR55 agonist structures lack the pendant phenyl or heterocyclic ring found in the antagonist structures after the central portion. Instead, agonist structures maintain a thin vertical profile in the binding pocket. This pendant portion in ML193, ML192, and ML191 may be able to block putative toggle switch residues M3.36(104) and F6.48(239) from undergoing any conformational change, providing one means by which these compounds may function as antagonists. Second, the locations of the highest negative electrostatic potential regions of the two classes deviate from each other. The agonists have their most electronegative region [which hydrogen bonds to K2.60(80)] near the broad head region, while the most electronegative region found in antagonists is near the end of the central portion of the molecule. Because K2.60(80) is located two turns from the extracellular end of the GPR55 TMH bundle, the GPR55 antagonists studied here bind higher than GPR55 agonists, extending into the EC loop region. The EC-2 loop residue, F169, for example is an important interaction site for ML191, ML192, and ML193. As discussed above, EC-2 loop conformational changes have been reported to be critical for signal transduction of numerous class A GPCRs. The fact that ML191, ML192, and ML193 all bind high enough in GPR55 to interact directly with and block movement of the EC-2 loop may be another reason for the antagonism exhibited by these compounds.

Future Directions. The diverse ML191, ML192, and ML193 chemotypes together with knowledge of the key GPR55 binding pocket interaction sites identified here should stimulate the creation of more potent and efficacious next-generation ligands with GPR55 selectivity. Such studies are underway in our laboratories. For example, our modeling studies suggest that there is a pocket underneath the EC-2 loop above K2.60(80) and next to C3.25(94) of which the first-generation antagonists do not take advantage. This region is partly hydrophobic [L2.63(83), V3.28(97), and M(167)] and partly hydrophilic [K2.60(80) and E3.29(98)]. In addition, mutational studies currently underway include mutations to test the effects of key amino acids in the ligand pocket, including the M3.36(104)−F6.48(239) toggle switch.

■ ASSOCIATED CONTENT

Supporting Information

Tables of interaction energies for each GPR55−ligand complex reported here (Tables S.1−S.7), Glide scores and conformational cost for each antagonist−receptor complex (Table S.9), rmsd values for docked ligands relative to their global minima (Table S.10), results from molecular dynamics simulations (Figures S.1−S.12 and Table S.11), the dock of CID16020046 with GPR55 R (Figure S.13), the dock of CBD with GPR55 R (Figure S.14), the dock of 3-(2-hydroxybenzyl)-5-isopropyl-8-methyl-2*H*-chromen-2-one with GPR55 R (Figure S.15), and the dock of tetrahydromagnolol with GPR55 R (Figure S.16). This material is available free of charge via the Internet at http://pubs.acs.org.

■ AUTHOR INFORMATION

Corresponding Author

*Center for Drug Discovery, University of North Carolina, Greensboro, NC 27402. E-mail: phreggio@uncg.edu. Phone: (336) 334-5333. Fax: (336) 334-5402.

Author Contributions

E.K., H.S., and D.M.S. contributed equally to this work. M.E.A. and P.H.R. also contributed equally to this work.

Funding

This research was supported by National Institutes of Health Grants DA029432, DA022950, DA021358, DA023204, NS077347, and P30DA013429. The HCS screening portion of this work was supported by National Institutes of Health Roadmap Program Grant U54HG005033 and performed at Sanford-Burnham Medical Research Institute's Conrad Prebys Center for Chemical Genomics (CPCCG), a comprehensive screening center with an X01 DA026205 grant to M.E.A.

Notes

The authors declare no competing financial interest.

■ ACKNOWLEDGMENTS

We acknowledge Drs. Russell Dahl and Shenghua Shi for selecting compounds from the primary screen for further testing.

■ ABBREVIATIONS

β_2-AR, β_2-adrenergic receptor; CB1, cannabinoid type 1 receptor; CB2, cannabinoid type 2 receptor; CM, Conformational Memories; EC, extracellular; ERK, extracellular regulated kinase; GFP, Green Fluorescent Protein; GPCR, G protein-coupled receptor; IC, intracellular; LP, lone pair of electrons; LPI, lysophosphatidylinositol; MAPK, mitogen-activated pro-

tein kinase; ML186 (CID15945391), *N*-(2-methoxy-5-morpholin-4-ylsulfonylphenyl)-4,5,6,7-tetrahydro-1-benzothiophene-2-carboxamide; ML191 (CID 23612552), 5-phenyl-3-{1-[1-(*p*-tolyl)cyclopropylcarbonyl]piperidin-4-yl}-1,3,4-oxadiazol-2(3*H*)-one; ML192 (CID 1434953), furan-2-yl[4-(2-methyl-5,6,7,8-tetrahydrobenzo[4,5]thieno[2,3-*d*]pyrimidin-4-yl)-piperazin-1-yl]methanone; ML193 (CID 1261822), *N*-{4-[*N*-(3,4-dimethylisoxazol-5yl)sulfamoyl]phenyl}-6,8-dimethyl-2-(pyridin-2-yl)quinoline-4-carboxamide; MLPCN, Molecular Libraries Probe Production Centers Network; TMH, transmembrane helix.

REFERENCES

(1) Henstridge, C. M., Balenga, N. A., Kargl, J., Andradas, C., Brown, A. J., Irving, A., Sanchez, C., and Waldhoer, M. (2011) Minireview: Recent Developments in the Physiology and Pathology of the Lysophosphatidylinositol-Sensitive Receptor GPR55. *Mol. Endocrinol. 25*, 1835−1848.

(2) Staton, P. C., Hatcher, J. P., Walker, D. J., Morrison, A. D., Shapland, E. M., Hughes, J. P., Chong, E., Mander, P. K., Green, P. J., Billinton, A., Fulleylove, M., Lancaster, H. C., Smith, J. C., Bailey, L. T., Wise, A., Brown, A. J., Richardson, J. C., and Chessell, I. P. (2008) The putative cannabinoid receptor GPR55 plays a role in mechanical hyperalgesia associated with inflammatory and neuropathic pain. *Pain 139*, 225−236.

(3) Whyte, L. S., Ryberg, E., Sims, N. A., Ridge, S. A., Mackie, K., Greasley, P. J., Ross, R. A., and Rogers, M. J. (2009) The putative cannabinoid receptor GPR55 affects osteoclast function in vitro and bone mass in vivo. *Proc. Natl. Acad. Sci. U.S.A. 106*, 16511−16516.

(4) Ford, L. A., Roelofs, A. J., Anavi-Goffer, S., Mowat, L., Simpson, D. G., Irving, A. J., Rogers, M. J., Rajnicek, A. M., and Ross, R. A. (2010) A role for L-α-lysophosphatidylinositol and GPR55 in the modulation of migration, orientation and polarization of human breast cancer cells. *Br. J. Pharmacol. 160*, 762−771.

(5) Andradas, C., Caffarel, M. M., Perez-Gomez, E., Salazar, M., Lorente, M., Velasco, G., Guzman, M., and Sanchez, C. (2011) The orphan G protein-coupled receptor GPR55 promotes cancer cell proliferation via ERK. *Oncogene 30*, 245−252.

(6) Perez-Gomez, E., Andradas, C., Flores, J. M., Quintanilla, M., Paramio, J. M., Guzman, M., and Sanchez, C. (2013) The orphan receptor GPR55 drives skin carcinogenesis and is upregulated in human squamous cell carcinomas. *Oncogene 32*, 2534−2542.

(7) Pineiro, R., Maffucci, T., and Falasca, M. (2011) The putative cannabinoid receptor GPR55 defines a novel autocrine loop in cancer cell proliferation. *Oncogene 30*, 142−152.

(8) Sharir, H., and Abood, M. E. (2010) Pharmacological characterization of GPR55, a putative cannabinoid receptor. *Pharmacol. Ther. 126*, 301−313.

(9) Anavi-Goffer, S., Baillie, G., Irving, A. J., Gertsch, J., Greig, I. R., Pertwee, R. G., and Ross, R. A. (2012) Modulation of L-α-lysophosphatidylinositol/GPR55 mitogen-activated protein kinase (MAPK) signaling by cannabinoids. *J. Biol. Chem. 287*, 91−104.

(10) Heynen-Genel, S., Dahl, R., Shi, S., Milan, L., Hariharan, S., Bravo, Y., Sergienko, E., Hedrick, M., Dad, S., Stonich, D., Su, Y., Vicchiarelli, M., Mangravita-Novo, A., Smith, L. H., Chung, T. D. Y., Sharir, H., Barak, L. S., and Abood, M. E. (2010) Screening for Selective Ligands for GPR55: Agonists. In Probe Reports from the NIH Molecular Libraries Program, National Institutes of Health, Bethesda, MD.

(11) Heynen-Genel, S., Dahl, R., Shi, S., Milan, L., Hariharan, S., Sergienko, E., Hedrick, M., Dad, S., Stonich, D., Su, Y., Vicchiarelli, M., Mangravita-Novo, A., Smith, L. H., Chung, T. D. Y., Sharir, H., Caron, M. G., Barak, L. S., and Abood, M. E. (2010) Screening for Selective Ligands for GPR55: Antagonists. In Probe Reports from the NIH Molecular Libraries Program, National Institutes of Health, Bethesda, MD.

(12) Brown, A. J., Daniels, D. A., Kassim, M., Brown, S., Haslam, C. P., Terrell, V. R., Brown, J., Nichols, P. L., Staton, P. C., Wise, A., and Dowell, S. J. (2011) Pharmacology of GPR55 in yeast and identification of GSK494581A as a mixed-activity glycine transporter subtype 1 inhibitor and GPR55 agonist. *J. Pharmacol. Exp. Ther. 337*, 236−246.

(13) Yin, H., Chu, A., Li, W., Wang, B., Shelton, F., Otero, F., Nguyen, D. G., Caldwell, J. S., and Chen, Y. A. (2009) Lipid G protein-coupled receptor ligand identification using β-arrestin PathHunter assay. *J. Biol. Chem. 284*, 12328−12338.

(14) Chun, E., Thompson, A. A., Liu, W., Roth, C. B., Griffith, M. T., Katritch, V., Kunken, J., Xu, F., Cherezov, V., Hanson, M. A., and Stevens, R. C. (2012) Fusion partner toolchest for the stabilization and crystallization of G protein-coupled receptors. *Structure 20*, 967−976.

(15) Kapur, A., Zhao, P., Sharir, H., Bai, Y., Caron, M. G., Barak, L. S., and Abood, M. E. (2009) Atypical responsiveness of the orphan receptor GPR55 to cannabinoid ligands. *J. Biol. Chem. 284*, 29817−29827.

(16) Sharir, H., Console-Bram, L., Mundy, C., Popoff, S. N., Kapur, A., and Abood, M. E. (2012) The endocannabinoids anandamide and virodhamine modulate the activity of the candidate cannabinoid receptor GPR55. *Journal of Neuroimmune Pharmacology 7*, 856−865.

(17) Kotsikorou, E., Madrigal, K. E., Hurst, D. P., Sharir, H., Lynch, D. L., Heynen-Genel, S., Milan, L. B., Chung, T. D., Seltzman, H. H., Bai, Y., Caron, M. G., Barak, L., Abood, M. E., and Reggio, P. H. (2011) Identification of the GPR55 agonist binding site using a novel set of high-potency GPR55 selective ligands. *Biochemistry 50*, 5633−5647.

(18) Cherezov, V., Rosenbaum, D. M., Hanson, M. A., Rasmussen, S. G., Thian, F. S., Kobilka, T. S., Choi, H. J., Kuhn, P., Weis, W. I., Kobilka, B. K., and Stevens, R. C. (2007) High-resolution crystal structure of an engineered human β2-adrenergic G protein-coupled receptor. *Science 318*, 1258−1265.

(19) Wu, B., Chien, E. Y., Mol, C. D., Fenalti, G., Liu, W., Katritch, V., Abagyan, R., Brooun, A., Wells, P., Bi, F. C., Hamel, D. J., Kuhn, P., Handel, T. M., Cherezov, V., and Stevens, R. C. (2010) Structures of the CXCR4 Chemokine GPCR with Small-Molecule and Cyclic Peptide Antagonists. *Science 330*, 1066−1071.

(20) Henstridge, C. M., Balenga, N. A., Schroder, R., Kargl, J. K., Platzer, W., Martini, L., Arthur, S., Penman, J., Whistler, J. L., Kostenis, E., Waldhoer, M., and Irving, A. J. (2010) GPR55 ligands promote receptor coupling to multiple signalling pathways. *Br. J. Pharmacol. 160*, 604−614.

(21) Feng, X., Zhang, J., Barak, L. S., Meyer, T., Caron, M. G., and Hannun, Y. A. (1998) Visualization of dynamic trafficking of a protein kinase C βII/green fluorescent protein conjugate reveals differences in G protein-coupled receptor activation and desensitization. *J. Biol. Chem. 273*, 10755−10762.

(22) Li, J., Edwards, P. C., Burghammer, M., Villa, C., and Schertler, G. F. (2004) Structure of Bovine Rhodopsin in a Trigonal Crystal Form. *J. Mol. Biol. 3443*, 1429−1438.

(23) Okada, T., Fujiyoshi, Y., Silow, M., Navarro, J., Landau, E. M., and Shichida, Y. (2002) Functional role of internal water molecules in rhodopsin revealed by X-ray crystallography. *Proc. Natl. Acad. Sci. U.S.A. 99*, 5982−5987.

(24) Palczewski, K., Kumasaka, T., Hori, T., Behnke, C. A., Motoshima, H., Fox, B. A., Le Trong, I., Teller, D. C., Okada, T., Stenkamp, R. E., Yamamoto, M., and Miyano, M. (2000) Crystal structure of rhodopsin: A G protein-coupled receptor. *Science 289*, 739−745.

(25) Shi, L., Liapakis, G., Xu, R., Guarnieri, F., Ballesteros, J. A., and Javitch, J. A. (2002) Beta2 adrenergic receptor activation. Modulation of the proline kink in transmembrane 6 by a rotamer toggle switch. *J. Biol. Chem. 277* (43), 40989−40996.

(26) McAllister, S. D., Hurst, D. P., Barnett-Norris, J., Lynch, D., Reggio, P. H., and Abood, M. E. (2004) Structural mimicry in class A G protein-coupled receptor rotamer toggle switches: The importance of the F3.36(201)/W6.48(357) interaction in cannabinoid CB1 receptor activation. *J. Biol. Chem. 279*, 48024−48037.

(27) Rosenbaum, D. M., Zhang, C., Lyons, J. A., Holl, R., Aragao, D., Arlow, D. H., Rasmussen, S. G., Choi, H. J., Devree, B. T., Sunahara, R.

K., Chae, P. S., Gellman, S. H., Dror, R. O., Shaw, D. E., Weis, W. I., Caffrey, M., Gmeiner, P., and Kobilka, B. K. (2011) Structure and function of an irreversible agonist-β_2 adrenoceptor complex. *Nature 469*, 236−240.

(28) Hamm, H. E., Deretic, D., Arendt, A., Hargrave, P. A., Koenig, B., and Hofmann, K. P. (1988) Site of G protein binding to rhodopsin mapped with synthetic peptides from the α subunit. *Science 241*, 832−835.

(29) Rasmussen, S. G., DeVree, B. T., Zou, Y., Kruse, A. C., Chung, K. Y., Kobilka, T. S., Thian, F. S., Chae, P. S., Pardon, E., Calinski, D., Mathiesen, J. M., Shah, S. T., Lyons, J. A., Caffrey, M., Gellman, S. H., Steyaert, J., Skiniotis, G., Weis, W. I., Sunahara, R. K., and Kobilka, B. K. (2011) Crystal structure of the β2 adrenergic receptor-Gs protein complex. *Nature 477*, 549−555.

(30) Farrens, D. L., Altenbach, C., Yang, K., Hubbell, W. L., and Khorana, H. G. (1996) Requirement of Rigid-Body Motion of Transmembrane Helicies for Light-Activation of Rhodopsin. *Science 274*, 768−770.

(31) Ghanouni, P., Steenhuis, J. J., Farrens, D., and Kobilka, B. (2001) Agonist Induced conformational Changes in the G-Protein Coupling Domain of the β-2-Adrenergic Receptor. *Proc. Natl. Acad. Sci. U.S.A. 98*, 5997−6002.

(32) Javitch, J. A., Fu, D., Liapakis, G., and Chen, J. (1997) Constitutive activation of the β2 adrenergic receptor alters the orientation of its sixth membrane-spanning segment. *J. Biol. Chem. 272*, 18546−18549.

(33) Jensen, A. D., Guarnieri, F., Rasmussen, S. G., Asmar, F., Ballesteros, J. A., and Gether, U. (2001) Agonist-induced conformational changes at the cytoplasmic side of transmembrane segment 6 in the β2 adrenergic receptor mapped by site-selective fluorescent labeling. *J. Biol. Chem. 276*, 9279−9290.

(34) Lin, S. W., and Sakmar, T. P. (1996) Specific tryptophan UV-absorbance changes are probes of the transition of rhodopsin to its active state. *Biochemistry 35*, 11149−11159.

(35) Nakanishi, J., Takarada, T., Yunoki, S., Kikuchi, Y., and Maeda, M. (2006) FRET-based monitoring of conformational change of the β2 adrenergic receptor in living cells. *Biochem. Biophys. Res. Commun. 343*, 1191−1196.

(36) Ballesteros, J. A., Jensen, A. D., Liapakis, G., Rasmussen, S. G., Shi, L., Gether, U., and Javitch, J. A. (2001) Activation of the β2-adrenergic receptor involves disruption of an ionic lock between the cytoplasmic ends of transmembrane segments 3 and 6. *J. Biol. Chem. 276*, 29171−29177.

(37) Standfuss, J., Edwards, P. C., D'Antona, A., Fransen, M., Xie, G., Oprian, D. D., and Schertler, G. F. (2011) The structural basis of agonist-induced activation in constitutively active rhodopsin. *Nature 471*, 656−660.

(38) McAllister, S. D., Rizvi, G., Anavi-Goffer, S., Hurst, D. P., Barnett-Norris, J., Lynch, D. L., Reggio, P. H., and Abood, M. E. (2003) An Aromatic Microdomain at the Cannabinoid CB(1) Receptor Constitutes an Agonist/Inverse Agonist Binding Region. *J. Med. Chem. 46*, 5139−5152.

(39) Hurst, D. P., Grossfield, A., Lynch, D. L., Feller, S., Romo, T. D., Gawrisch, K., Pitman, M. C., and Reggio, P. H. (2010) A lipid pathway for ligand binding is necessary for a cannabinoid G protein-coupled receptor. *J. Biol. Chem. 285*, 17954−17964.

(40) Lynch, D., Hurst, D., Romo, T., Grossfield, A., Reggio, P., and Pitman, M. (2012) Characterizing the Motion of W6.48 in the Active State of a GPCR. *2012 Biophysical Society Meeting Abstracts*, Biophysical Journal Supplement, Biophysical Society, Rockville, MD.

(41) Ahuja, S., Hornak, V., Yan, E. C., Syrett, N., Goncalves, J. A., Hirshfeld, A., Ziliox, M., Sakmar, T. P., Sheves, M., Reeves, P. J., Smith, S. O., and Eilers, M. (2009) Helix movement is coupled to displacement of the second extracellular loop in rhodopsin activation. *Nat. Struct. Mol. Biol. 16*, 168−175.

(42) Unal, H., Jagannathan, R., Bhat, M. B., and Karnik, S. S. (2010) Ligand-specific conformation of extracellular loop-2 in the angiotensin II type 1 receptor. *J. Biol. Chem. 285*, 16341−16350.

(43) Unal, H., Jagannathan, R., Bhatnagar, A., Tirupula, K., Desnoyer, R., and Karnik, S. S. (2013) Long Range Effect of Mutations on Specific Conformational Changes in the Extracellular Loop 2 of Angiotensin II Type 1 Receptor. *J. Biol. Chem. 288*, 540−551.

(44) Baneres, J. L., Mesnier, D., Martin, A., Joubert, L., Dumuis, A., and Bockaert, J. (2005) Molecular characterization of a purified 5-HT4 receptor: A structural basis for drug efficacy. *J. Biol. Chem. 280*, 20253−20260.

(45) Ahn, K. H., Bertalovitz, A. C., Mierke, D. F., and Kendall, D. A. (2009) Dual role of the second extracellular loop of the cannabinoid receptor 1: Ligand binding and receptor localization. *Mol. Pharmacol. 76*, 833−842.

(46) Bertalovitz, A. C., Ahn, K. H., and Kendall, D. A. (2010) Ligand Binding Sensitivity of the Extracellular Loop Two of the Cannabinoid Receptor 1. *Drug Dev. Res. 71*, 404−411.

(47) Rempel, V., Volz, N., Glaser, F., Nieger, M., Brase, S., and Muller, C. E. (2013) Antagonists for the Orphan G-Protein-Coupled Receptor GPR55 Based on a Coumarin Scaffold. *J. Med. Chem. 56*, 4798−4810.

(48) Kargl, J., Brown, A. J., Andersen, L., Dorn, G., Schicho, R., Waldhoer, M., and Heinemann, A. (2013) A selective antagonist reveals a potential role of G protein-coupled receptor 55 in platelet and endothelial cell function. *J. Pharmacol. Exp. Ther. 346*, 54−66.

(49) Rempel, V., Fuchs, A., Hinz, S., Karcz, T., Lehr, M., Koetter, U., and Müller, C. (2013) Magnolia Extract, Magnolol, and Metabolites: Activation of Cannabinoid CB2 Receptors and Blockade of the Related GPR55. *ACS Med. Chem. Lett. 4*, 41−45.

(50) McHugh, D., Hu, S. S., Rimmerman, N., Juknat, A., Vogel, Z., Walker, J. M., and Bradshaw, H. B. (2010) N-arachidonoyl glycine, an abundant endogenous lipid, potently drives directed cellular migration through GPR18, the putative abnormal cannabidiol receptor. *BMC Neurosci. 11*, 44.